

PDF hosted at the Radboud Repository of the Radboud University Nijmegen

The following full text is a preprint version which may differ from the publisher's version.

For additional information about this publication click this link.

<http://hdl.handle.net/2066/124591>

Please be advised that this information was generated on 2021-09-22 and may be subject to change.

Measurement of the mass of the W boson in e^+e^- collisions at $\sqrt{s} = 161$ GeV

The OPAL Collaboration

Abstract

This letter describes the first observation of W boson pair production at a centre-of-mass energy $\sqrt{s} = 161.3$ GeV in the OPAL detector at LEP. The analysis is sensitive to all expected W^+W^- decay channels. A total of 28 events have been selected for an integrated luminosity of 9.89 ± 0.06 pb $^{-1}$. This is consistent with the Standard Model expectation, including signal and background contributions. The W pair production cross-section is measured to be $\sigma_{WW} = 3.62_{-0.82}^{+0.93} \pm 0.16$ pb. An analysis of the predicted M_W dependence of the accepted cross-section, taking into account interference in the four-fermion production processes, yields $M_W = 80.40_{-0.41-0.10}^{+0.44+0.09} \pm 0.10$ GeV, where the first and second uncertainties are statistical and systematic, respectively, and the third arises from the beam energy uncertainty.

(Submitted to Physics Letters B)

The OPAL Collaboration

K. Ackerstaff⁸, G. Alexander²³, J. Allison¹⁶, N. Altekamp⁵, K. Ametewee²⁵, K.J. Anderson⁹, S. Anderson¹², S. Arcelli², S. Asai²⁴, D. Axen²⁹, G. Azuelos^{18,a}, A.H. Ball¹⁷, E. Barberio⁸, R.J. Barlow¹⁶, R. Bartoldus³, J.R. Batley⁵, J. Bechtluft¹⁴, C. Beeston¹⁶, T. Behnke⁸, A.N. Bell¹, K.W. Bell²⁰, G. Bella²³, S. Bentvelsen⁸, P. Berlich¹⁰, S. Bethke¹⁴, O. Biebel¹⁴, V. Blobel²⁷, I.J. Bloodworth¹, J.E. Bloomer¹, M. Bobinski¹⁰, P. Bock¹¹, H.M. Bosch¹¹, M. Boutemour³⁴, B.T. Bouwens¹², S. Braibant¹², R.M. Brown²⁰, H.J. Burckhart⁸, C. Burgard⁸, R. Bürgin¹⁰, P. Capiluppi², R.K. Carnegie⁶, A.A. Carter¹³, J.R. Carter⁵, C.Y. Chang¹⁷, D.G. Charlton^{1,b}, D. Chrisman⁴, P.E.L. Clarke¹⁵, I. Cohen²³, J.E. Conboy¹⁵, O.C. Cooke¹⁶, M. Cuffiani², S. Dado²², C. Dallapiccola¹⁷, G.M. Dallavalle², S. De Jong¹², L.A. del Pozo⁸, K. Desch³, M.S. Dixit⁷, E. do Couto e Silva¹², M. Doucet¹⁸, E. Duchovni²⁶, G. Duckeck³⁴, I.P. Duerdoth¹⁶, J.E.G. Edwards¹⁶, P.G. Estabrooks⁶, H.G. Evans⁹, M. Evans¹³, F. Fabbri², P. Fath¹¹, F. Fiedler²⁷, M. Fierro², H.M. Fischer³, R. Folman²⁶, D.G. Fong¹⁷, M. Foucher¹⁷, A. Fürtjes⁸, P. Gagnon⁷, J.W. Gary⁴, J. Gascon¹⁸, S.M. Gascon-Shotkin¹⁷, N.I. Geddes²⁰, C. Geich-Gimbel³, T. Gerals²⁰, G. Giacomelli², P. Giacomelli⁴, R. Giacomelli², V. Gibson⁵, W.R. Gibson¹³, D.M. Gingrich^{30,a}, D. Glenzinski⁹, J. Goldberg²², M.J. Goodrick⁵, W. Gorn⁴, C. Grandi², E. Gross²⁶, J. Grunhaus²³, M. Gruwé⁸, C. Hajdu³², G.G. Hanson¹², M. Hansroul⁸, M. Hapke¹³, C.K. Hargrove⁷, P.A. Hart⁹, C. Hartmann³, M. Hauschild⁸, C.M. Hawkes⁵, R. Hawkings⁸, R.J. Hemingway⁶, M. Herndon¹⁷, G. Herten¹⁰, R.D. Heuer⁸, M.D. Hildreth⁸, J.C. Hill⁵, S.J. Hillier¹, T. Hilse¹⁰, P.R. Hobson²⁵, R.J. Homer¹, A.K. Honma^{28,a}, D. Horváth^{32,c}, R. Howard²⁹, R.E. Hughes-Jones¹⁶, D.E. Hutchcroft⁵, P. Igo-Kemenes¹¹, D.C. Imrie²⁵, M.R. Ingram¹⁶, K. Ishii²⁴, A. Jawahery¹⁷, P.W. Jeffreys²⁰, H. Jeremie¹⁸, M. Jimack¹, A. Joly¹⁸, C.R. Jones⁵, G. Jones¹⁶, M. Jones⁶, R.W.L. Jones⁸, U. Jost¹¹, P. Jovanovic¹, T.R. Junk⁸, D. Karlen⁶, K. Kawagoe²⁴, T. Kawamoto²⁴, R.K. Keeler²⁸, R.G. Kellogg¹⁷, B.W. Kennedy²⁰, B.J. King⁸, J. Kirk²⁹, S. Kluth⁸, T. Kobayashi²⁴, M. Kobel¹⁰, D.S. Koetke⁶, T.P. Kokott³, M. Kolrep¹⁰, S. Komamiya²⁴, T. Kress¹¹, P. Krieger⁶, J. von Krogh¹¹, P. Kyberd¹³, G.D. Lafferty¹⁶, R. Lahmann¹⁷, W.P. Lai¹⁹, D. Lanske¹⁴, J. Lauber¹⁵, S.R. Lautenschlager³¹, J.G. Layter⁴, D. Lazic²², A.M. Lee³¹, E. Lefebvre¹⁸, D. Lellouch²⁶, J. Letts², L. Levinson²⁶, C. Lewis¹⁵, S.L. Lloyd¹³, F.K. Loebinger¹⁶, G.D. Long¹⁷, M.J. Losty⁷, J. Ludwig¹⁰, M. Mannelli⁸, S. Marcellini², C. Markus³, A.J. Martin¹³, J.P. Martin¹⁸, G. Martinez¹⁷, T. Mashimo²⁴, W. Matthews²⁵, P. Mättig³, W.J. McDonald³⁰, J. McKenna²⁹, E.A. Mckigney¹⁵, T.J. McMahon¹, A.I. McNab¹³, R.A. McPherson⁸, F. Meijers⁸, S. Menke³, F.S. Merritt⁹, H. Mes⁷, J. Meyer²⁷, A. Michelini², G. Mikenberg²⁶, D.J. Miller¹⁵, R. Mir²⁶, W. Mohr¹⁰, A. Montanari², T. Mori²⁴, M. Morii²⁴, U. Müller³, K. Nagai²⁶, I. Nakamura²⁴, H.A. Neal⁸, B. Nellen³, B. Nijhar¹⁶, R. Nisius⁸, S.W. O'Neale¹, F.G. Oakham⁷, F. Odorici², H.O. Ogren¹², N.J. Oldershaw¹⁶, T. Omori²⁴, M.J. Oreglia⁹, S. Orito²⁴, J. Pálkás^{33,d}, G. Pásztor³², J.R. Pater¹⁶, G.N. Patrick²⁰, J. Patt¹⁰, M.J. Pearce¹, S. Petzold²⁷, P. Pfeifenschneider¹⁴, J.E. Pilcher⁹, J. Pinfold³⁰, D.E. Plane⁸, P. Poffenberger²⁸, B. Poli², A. Posthaus³, H. Przysieciak³⁰, D.L. Rees¹, D. Rigby¹, S. Robertson²⁸, S.A. Robins¹³, N. Rodning³⁰, J.M. Roney²⁸, A. Rooke¹⁵, E. Ros⁸, A.M. Rossi², M. Rosvick²⁸, P. Routenburg³⁰, Y. Rozen²², K. Runge¹⁰, O. Runolfsson⁸, U. Ruppel¹⁴, D.R. Rust¹², R. Rylko²⁵, K. Sachs¹⁰, E.K.G. Sarkisyan²³, M. Sasaki²⁴, C. Sbarra², A.D. Schaile³⁴, O. Schaile³⁴, F. Scharf³, P. Scharff-Hansen⁸, P. Schenk²⁷, B. Schmitt⁸, S. Schmitt¹¹, M. Schröder⁸, H.C. Schultz-Coulon¹⁰, M. Schulz⁸, M. Schumacher³, P. Schütz³, W.G. Scott²⁰, T.G. Shears¹⁶, B.C. Shen⁴, C.H. Shepherd-Themistocleous⁸, P. Sherwood¹⁵, G.P. Siroli², A. Sittler²⁷, A. Skillman¹⁵, A. Skuja¹⁷, A.M. Smith⁸, T.J. Smith²⁸, G.A. Snow¹⁷, R. Sobie²⁸, S. Söldner-Rembold¹⁰, R.W. Springer³⁰, M. Sproston²⁰, A. Stahl³, M. Steiert¹¹, K. Stephens¹⁶, J. Steuerer²⁷, B. Stockhausen³, D. Strom¹⁹, F. Strumia⁸, P. Szymanski²⁰, R. Tafirout¹⁸, S.D. Talbot¹, S. Tanaka²⁴, P. Taras¹⁸, S. Tarem²², M. Thiergen¹⁰, M.A. Thomson⁸, E. von Törne³, S. Towers⁶, I. Trigger¹⁸, T. Tsukamoto²⁴, E. Tsur²³, A.S. Turcot⁹, M.F. Turner-Watson⁸, P. Utzat¹¹, R. Van Kooten¹², M. Verzocchi¹⁰, P. Vikas¹⁸, M. Vincter²⁸, E.H. Vokurka¹⁶, F. Wäckerle¹⁰, A. Wagner²⁷, C.P. Ward⁵, D.R. Ward⁵, J.J. Ward¹⁵, P.M. Watkins¹, A.T. Watson¹, N.K. Watson⁷, P.S. Wells⁸, N. Vermes³,

¹School of Physics and Space Research, University of Birmingham, Birmingham B15 2TT, UK

²Dipartimento di Fisica dell' Università di Bologna and INFN, I-40126 Bologna, Italy

³Physikalisches Institut, Universität Bonn, D-53115 Bonn, Germany

⁴Department of Physics, University of California, Riverside CA 92521, USA

⁵Cavendish Laboratory, Cambridge CB3 0HE, UK

⁶Ottawa-Carleton Institute for Physics, Department of Physics, Carleton University, Ottawa, Ontario K1S 5B6, Canada

⁷Centre for Research in Particle Physics, Carleton University, Ottawa, Ontario K1S 5B6, Canada

⁸CERN, European Organisation for Particle Physics, CH-1211 Geneva 23, Switzerland

⁹Enrico Fermi Institute and Department of Physics, University of Chicago, Chicago IL 60637, USA

¹⁰Fakultät für Physik, Albert Ludwigs Universität, D-79104 Freiburg, Germany

¹¹Physikalisches Institut, Universität Heidelberg, D-69120 Heidelberg, Germany

¹²Indiana University, Department of Physics, Swain Hall West 117, Bloomington IN 47405, USA

¹³Queen Mary and Westfield College, University of London, London E1 4NS, UK

¹⁴Technische Hochschule Aachen, III Physikalisches Institut, Sommerfeldstrasse 26-28, D-52056 Aachen, Germany

¹⁵University College London, London WC1E 6BT, UK

¹⁶Department of Physics, Schuster Laboratory, The University, Manchester M13 9PL, UK

¹⁷Department of Physics, University of Maryland, College Park, MD 20742, USA

¹⁸Laboratoire de Physique Nucléaire, Université de Montréal, Montréal, Quebec H3C 3J7, Canada

¹⁹University of Oregon, Department of Physics, Eugene OR 97403, USA

²⁰Rutherford Appleton Laboratory, Chilton, Didcot, Oxfordshire OX11 0QX, UK

²²Department of Physics, Technion-Israel Institute of Technology, Haifa 32000, Israel

²³Department of Physics and Astronomy, Tel Aviv University, Tel Aviv 69978, Israel

²⁴International Centre for Elementary Particle Physics and Department of Physics, University of Tokyo, Tokyo 113, and Kobe University, Kobe 657, Japan

²⁵Brunel University, Uxbridge, Middlesex UB8 3PH, UK

²⁶Particle Physics Department, Weizmann Institute of Science, Rehovot 76100, Israel

²⁷Universität Hamburg/DESY, II Institut für Experimental Physik, Notkestrasse 85, D-22607 Hamburg, Germany

²⁸University of Victoria, Department of Physics, P O Box 3055, Victoria BC V8W 3P6, Canada

²⁹University of British Columbia, Department of Physics, Vancouver BC V6T 1Z1, Canada

³⁰University of Alberta, Department of Physics, Edmonton AB T6G 2J1, Canada

³¹Duke University, Dept of Physics, Durham, NC 27708-0305, USA

³²Research Institute for Particle and Nuclear Physics, H-1525 Budapest, P O Box 49, Hungary

³³Institute of Nuclear Research, H-4001 Debrecen, P O Box 51, Hungary

³⁴Ludwigs-Maximilians-Universität München, Sektion Physik, Am Coulombwall 1, D-85748 Garching, Germany

^a and at TRIUMF, Vancouver, Canada V6T 2A3

^b and Royal Society University Research Fellow

^c and Institute of Nuclear Research, Debrecen, Hungary

^d and Department of Experimental Physics, Lajos Kossuth University, Debrecen, Hungary

1 Introduction

In the initial phase of operation of LEP2, a centre-of-mass energy of $\sqrt{s} \simeq 161$ GeV has been attained for the first time in e^+e^- collisions. This centre-of-mass energy lies just above the W pair production threshold [1]. The cross-section for the process $e^+e^- \rightarrow W^+W^-$ increases rapidly with \sqrt{s} at centre-of-mass energies close to the nominal threshold of $\sqrt{s} = 2M_W$, where M_W is the mass of the W boson. However, the abrupt turn-on of the Born cross-section is distorted by the effects of the W width, initial state radiation and other electroweak corrections [3,4]. In this threshold region, the cross-section at a given value of \sqrt{s} has a particularly strong dependence on the value of M_W , and therefore it is possible to extract M_W from the data by measuring the cross-section and comparing with theoretical predictions in the context of the Standard Model. Such measurements of the mass of the W boson are complementary to those at $\bar{p}p$ colliders (currently $M_W = 80.33 \pm 0.15$ GeV [1], [2]) and to those which will be performed during later phases of LEP2 operation by reconstructing directly the decay products of the W. The LEP2 W mass measurements at threshold and at higher energies have rather different systematic uncertainties and a comparable statistical power for a given integrated luminosity [4].

This letter describes selections to identify W^+W^- production in all expected decay topologies¹ with the OPAL detector. Strict criteria are required to isolate the signal, as the expected cross-sections for W^+W^- production and the dominant background from $Z^0/\gamma \rightarrow f\bar{f}$, where f is any charged fermion, are on the order of 3 pb and 200 pb, respectively. In addition, backgrounds also arise from other processes with four-fermion intermediate states which do not contain two resonating W bosons. These four-fermion backgrounds fall into two classes: those which can interfere with the four-fermion states from W^+W^- production, and those which cannot. The interfering four-fermion backgrounds are particularly problematic because they can also depend on the W boson mass. This mass-dependent four-fermion background is taken into account in the determination of the W mass described in this letter. In addition, the cross-section of W pair production from the three doubly resonant W^+W^- production graphs (“CC03 diagrams” [3]) is measured from the data. This latter measurement assumes that the effects of interference in the accepted cross-section are small, which is expected to be a good approximation at the current level of statistical precision.

2 Data and Simulated Event Samples

This analysis uses the data recorded during the 1996 LEP run at 161 GeV by the OPAL detector, which is described fully elsewhere [5,6]. Charged tracks and electromagnetic calorimeter clusters are selected as in [7], the gamma catcher and forward calorimeters close to the beam axis² use the criteria given in [8], and clusters in the hadronic calorimeter are required to have an energy greater than 0.25 GeV. The accepted integrated luminosity, evaluated using forward Bhabha scattering events observed in the silicon tungsten forward calorimeter, is $9.890 \pm 0.042(\text{stat.}) \pm 0.040(\text{syst.}) \text{ pb}^{-1}$. The luminosity determination is slightly modified relative to that in [9] due to the introduction of protective shields in the forward regions.

In evaluating systematic uncertainties in the analyses described in this letter, extensive use is made of data and simulated events at $\sqrt{s} = 133$ GeV, of the high statistics samples at $\sqrt{s} = 91$ GeV, and of background enriched samples at $\sqrt{s} = 161$ GeV. A variety of Monte Carlo models are used to estimate efficiencies and backgrounds, and all events include a full simulation of the OPAL detector [10]. Two approaches have been adopted, as summarised below.

¹Throughout this letter, a reference to W^+ or its decay products implicitly includes the charge conjugate states.

²The coordinate system is such that the origin is at the geometric centre of the detector, \hat{z} is parallel to the e^- beam direction; r is the coordinate normal to \hat{z} , θ is the polar angle with respect to \hat{z} and ϕ is the azimuthal angle around \hat{z} .

In the first approach, signal and background samples were generated separately. The main signal sample was obtained with PYTHIA [11] and was generated at $\sqrt{s} = 161$ GeV using the current world-average W boson mass of $M_W = 80.33$ GeV [1]. The W^+W^- cross-section for this sample is within 2% of that predicted by the GENTLE program [12]. The latter cross-section is 3.77 pb for the centre-of-mass energy $\sqrt{s} = 161.3 \pm 0.2$ GeV [13]. As GENTLE is more complete, it is used to calculate the signal cross-section which gives the expected number of W^+W^- events throughout this letter. More details are given in Section 7. Estimates of the different background processes are based primarily on the PYTHIA, grc4f [14], KORALZ [15], BHWIDE [16], PHOJET [17], Vermaseren [18] and NUNUGPV [19] generators. Other models [20–23] are used to give an estimate of the systematic uncertainties.

In the second approach, all four-fermion final states are considered collectively. The separation between signal and background processes is complicated by the interference between the W^+W^- production diagrams (class CC03 of [3]) and other four-fermion graphs. For example, the process $Z^0/\gamma \rightarrow q\bar{q}$ where a W^\pm is radiated off one of the quarks can interfere with $W^+W^- \rightarrow q\bar{q}\ell\bar{\nu}_\ell$ and $W^+W^- \rightarrow q\bar{q}q\bar{q}$ final states. The effect of interference is included by generating a sample of four-fermion final states (including W^+W^-) using grc4f. Other backgrounds are included using the generators listed above. Systematic uncertainties are assessed by comparing grc4f with EXCALIBUR [21] which also includes the effect of interference. In addition, grc4f and EXCALIBUR were used to generate samples corresponding to W^+W^- production alone.

3 $W^+W^- \rightarrow q\bar{q}q\bar{q}$ Event Selection

Approximately 46% of the W pairs produced are expected to decay in the $q\bar{q}q\bar{q}$ channel, which is characterised by four energetic, hadronic jets. The pair of jets associated with each W has a large invariant mass, and as the W bosons are produced with relatively low momentum near threshold, the jets often appear back-to-back in the detector. There is a large hadronic background from $Z^0/\gamma \rightarrow q\bar{q}$ events. Most of these are produced in association with energetic initial state photons, but non-radiative $Z^0/\gamma \rightarrow q\bar{q}$ events, especially those with hard gluon radiation producing four jets, are particularly difficult to distinguish from $W^+W^- \rightarrow q\bar{q}q\bar{q}$ production.

Selected events must be identified as hadronic final states [24], have at least six tracks and six electromagnetic clusters, and more than 50 GeV of measured energy using tracks, electromagnetic clusters and hadronic clusters. Tracks and calorimeter clusters are then combined into four jets using the k_\perp (“Durham”) [25] jet-finding algorithm, and the total momentum and energy of each of the jets are corrected for double-counting of energy [26].

Events having an energetic initial state photon in the detector are removed by demanding the energy of the most energetic electromagnetic cluster to be less than $0.71E_\gamma$, where E_γ is the expected energy of an initial state photon produced in association with a real Z^0 and seen in the detector ($E_\gamma = 54.7$ GeV at $\sqrt{s} = 161$ GeV). A well separated, four-jet topology is ensured by requiring events to have a value of the jet resolution parameter for the three- to four-jet transition, $y_{34} > 0.01$. Events are rejected if any jet contains no tracks, in order to remove poorly reconstructed jets and radiative events which satisfy the E_γ criterion above. The four-vectors of the jets are used in a kinematic fit, which imposes conservation of energy and momentum and equality of the masses of the two jet pairs forming the W candidates. At least one of the three possible assignments of jets to W candidates must yield a fitted mass of more than 72 GeV, with a corresponding fit probability of at least 1%. These requirements remove more than 99% of the $Z^0/\gamma \rightarrow q\bar{q}$ background.

Distributions of the kinematic fit mass and y_{34} variables are shown in Figure 1 (a) and (b) for data and Monte Carlo, after all other cuts. The number of candidate events selected and the corresponding Monte Carlo expectations for signal and background events are given in Table 1. The background is

dominated by $Z^0/\gamma \rightarrow q\bar{q}$ events. The efficiency for selecting $W^+W^- \rightarrow q\bar{q}q\bar{q}$ events is estimated to be $(56.7 \pm 0.5)\%$.

The systematic uncertainty of 0.5% on the selection efficiency is estimated by comparing simulated W^+W^- events from a variety of models [11, 20–22], and by varying the fragmentation parameters within PYTHIA. The fractional systematic uncertainty of 11.3% on the accepted background cross-section is estimated by comparing different Monte Carlo models [11, 22, 23], high statistics LEP1 data with that simulated by JETSET [11], and by varying the fragmentation modelling within PYTHIA. A consistent background estimate is obtained from the relatively small $\sqrt{s} = 133$ GeV data sample. The systematic uncertainties of both selection efficiency and accepted background cross-section include a component from finite Monte Carlo statistics.

4 $W^+W^- \rightarrow q\bar{q}e\bar{\nu}_e$ and $W^+W^- \rightarrow q\bar{q}\mu\bar{\nu}_\mu$ Event Selection

Approximately 29% of W pairs produced are expected to decay in the $q\bar{q}e\bar{\nu}_e$ and $q\bar{q}\mu\bar{\nu}_\mu$ channels, which contain an energetic charged lepton (e or μ), two or more hadronic jets and missing momentum because of the unobserved neutrino. There is a substantial $Z^0/\gamma \rightarrow q\bar{q}$ background in which a hadron or an initial state photon is misidentified as a lepton. Four-fermion processes such as $Z^0e^+e^-$, $W\bar{\nu}_e$ and off-shell Z^0Z^0 production can lead to two hadronic jets and one identified lepton being observed in the detector, and thus constitute another source of background.

Purely leptonic final states are removed by requiring at least six tracks and at least eight electromagnetic calorimeter clusters per event. A muon candidate is a track which has associated hits in the muon chambers or the hadron calorimeter, and has only a small energy deposit in the electromagnetic calorimeter. Electrons are identified by requiring a tight match between the measured ϕ coordinate of a track and electromagnetic cluster, by removing tracks consistent with photon conversions, and by requiring the ionisation energy loss, dE/dx , and the ratio of the electromagnetic cluster energy, E , to the track momentum, p , to be consistent with the expectation for an electron. Rejecting candidates with significant associated hadronic activity beyond the electromagnetic calorimeter further enhances the purity of the $q\bar{q}e\bar{\nu}_e$ sample.

As the lepton candidate should be energetic, muons are required to have momentum $p > 20$ GeV, and electrons to have energy $E > 25$ GeV. In the region $|\cos\theta| > 0.90$, residual photon conversion background is reduced by insisting that electron candidates also satisfy $p > 25$ GeV. The lepton candidate must be isolated, *i.e.* $I \equiv \sum E + \sum |p| < 2.5$ GeV, where the sum includes all tracks and clusters within a 200 mrad cone around the lepton track, excluding the cluster associated with the track. To remove events containing $Z^0 \rightarrow \ell^+\ell^-$ decays, lepton candidates are rejected if their invariant mass together with any other track is within 10 GeV of the Z^0 mass. The total visible energy and momentum of the event, $(E_{\text{vis}}, \vec{p}_{\text{vis}})$, are evaluated using the algorithm of [26] for the hadronic system, and adding the four-momentum of the lepton candidate.

$W^+W^- \rightarrow q\bar{q}\ell\bar{\nu}_\ell$ events have a high momentum neutrino, and therefore have missing momentum and a reduced visible energy. Radiative Z^0/γ background events and singly resonant gauge boson events tend to have missing momentum along the beam direction, whereas the signal events normally have an unbalanced momentum in the $r - \phi$ plane. The following criteria exploit these characteristics, and also allow for the higher background in the $q\bar{q}e\bar{\nu}_e$ channel. Events are required to have a jet resolution scale in the k_\perp scheme for the two- to three-jet transition, $y_{23} > 0.005$, evaluated using tracks and unassociated electromagnetic clusters. The energy of the most energetic, isolated electromagnetic cluster must be less than $0.75E_\gamma$. Events are required to have a scaled missing momentum, $R_{\text{miss}} = |\vec{p}_{\text{miss}}|/\sqrt{s} > 0.07$, where $\vec{p}_{\text{miss}} = -\vec{p}_{\text{vis}}$. The scaled visible energy, $R_{\text{vis}} = E_{\text{vis}}/\sqrt{s}$, must lie in the interval $0.30 < R_{\text{vis}} < 1.00$ (0.95) where the lepton candidate is a muon (electron). The polar angle θ_{miss} of the missing momentum vector must be in the region given by $|\cos\theta_{\text{miss}}| < 0.95$. The $r - \phi$

components of the momentum vector \vec{p}_{vis} are used to calculate the total transverse momentum in the event, $\sum p_T$, which must be greater than 12 (16) GeV when the lepton candidate is a muon (electron).

Distributions of $\sum p_T$ and of the momenta of the selected lepton candidates are given in Figure 1 (c) and (d). The number of candidate events selected and the corresponding Monte Carlo expectations for signal and background events are given in Table 1. The selection efficiencies for the cuts listed above have been reduced by 2–3% to account for differences between Monte Carlo and data, determined using samples of “mixed” events, and by $\sim 1\%$ for modelling of final state radiation. These samples of mixed events are constructed from $q\bar{q}$ and $\ell^+\ell^-$ events at $\sqrt{s} = 91$ GeV, in data and Monte Carlo, to emulate true $W^+W^- \rightarrow q\bar{q}\ell\bar{\nu}_\ell$ processes. The efficiencies for the $q\bar{q}e\bar{\nu}_e$ and $q\bar{q}\mu\bar{\nu}_\mu$ selections are $(71.4 \pm 2.6)\%$ and $(76.9 \pm 2.5)\%$, respectively. These efficiencies include $(5.9 \pm 0.5)\%$ of the $q\bar{q}\tau\bar{\nu}_\tau$ channel that are selected by this analysis. The background is dominated by $Z^0/\gamma \rightarrow q\bar{q}$ and four-fermion processes, where the latter is estimated as the difference between the accepted cross-sections for full four-fermion and W^+W^- Monte Carlo samples.

The systematic uncertainty of approximately 2.5% on the selection efficiency in each channel includes contributions from comparisons of data and Monte Carlo using the samples of mixed events and of W^+W^- events simulated using different models [11, 14, 20, 21]. The systematic uncertainties on the small accepted background cross-sections are estimated by comparing the grc4f and EXCALIBUR predictions of the four-fermion background. The corresponding uncertainties from $Z^0/\gamma \rightarrow q\bar{q}$ are obtained by comparing the predictions of different models [11, 22, 23], and high statistics LEP1 data with that simulated by JETSET. A consistent background estimate is obtained from the $\sqrt{s} = 133$ GeV data sample, as in Section 3. The systematic uncertainties of both signal efficiency and accepted background cross-section include a component from finite Monte Carlo statistics, particularly for the four-fermion processes.

5 $W^+W^- \rightarrow q\bar{q}\tau\bar{\nu}_\tau$ Event Selection

Approximately 14% of W pairs produced are expected to decay in this partially leptonic mode, characterised by two or more hadronic jets, one τ decay jet and missing momentum associated with two or more neutrinos. The background is dominated by $Z^0/\gamma \rightarrow q\bar{q}$ events, where the third jet in the event is often due to either an initial state photon observed in the detector, or gluon emission. This analysis is also designed to select those $W^+W^- \rightarrow q\bar{q}e\bar{\nu}_e$ and $W^+W^- \rightarrow q\bar{q}\mu\bar{\nu}_\mu$ events which do not pass the strict lepton identification requirements described in Section 4.

Events must be identified as hadronic [24], consist of at least six tracks and eight electromagnetic clusters, and should not be selected as $W^+W^- \rightarrow q\bar{q}q\bar{q}$, $q\bar{q}e\bar{\nu}_e$ or $q\bar{q}\mu\bar{\nu}_\mu$. Three jets are formed in the event using the k_\perp algorithm and, in contrast to the $q\bar{q}\mu\bar{\nu}_\mu$ and $q\bar{q}e\bar{\nu}_e$ selections where a high energy charged lepton has been identified, the total energy and momentum of the entire event are corrected as in [26]. Events are required to satisfy the following: $|\cos\theta_{\text{miss}}| < 0.85$, $R_{\text{miss}} > 0.1$, $0.3 < R_{\text{vis}} < 0.9$ and $y_{23} > 0.005$, where the variables are as described in Section 4. In this case, as no lepton is explicitly identified, some of the criteria are slightly more restrictive. Requiring that all jets have at least one associated charged track removes events in which an energetic photon is reconstructed as a jet.

The pair of jets with the largest opening angle is assumed to be the $q\bar{q}$ pair from the hadronic W decay, leaving the remaining jet as the τ candidate. Monte Carlo studies of $W^+W^- \rightarrow q\bar{q}\tau\bar{\nu}_\tau$ events indicate that this assignment is correct in 75% of events. It fails when the τ is not well separated from one of the quark jets, or the W^+W^- pair is sufficiently off-shell that the decay products of the hadronically decaying W are no longer the most back-to-back pair of jets in the event. The jet assigned as the τ candidate is required to have either one or three tracks within 10° of the jet axis. It must also have less than 1.5 GeV of isolation energy, I , between 10° and 20° from the jet axis.

Distributions of $|\cos\theta_{\text{miss}}|$ and R_{vis} are given in Figure 2 (a) and (b). The number of candidate events selected and the corresponding Monte Carlo expectations for signal and background events are given in Table 1. Considering all W^+W^- events passing the $q\bar{q}\tau\bar{\nu}_\tau$ selection as signal gives an efficiency relative to the number of events expected from $W^+W^- \rightarrow q\bar{q}\tau\bar{\nu}_\tau$ of $(42.5 \pm 2.6)\%$. This efficiency has been increased as a consequence of the modelling corrections in the $q\bar{q}\bar{\nu}_e$ and $q\bar{q}\mu\bar{\nu}_\mu$ channels discussed in Section 4. The dominant systematic effect in the background estimate is due to the simulation of the isolation I . It includes a correction of $(+15 \pm 9)\%$ evaluated by comparing high statistics Z^0 data and Monte Carlo. The mixture of W -pair decay modes in the selected events is expected to be $q\bar{q}\bar{\nu}_e: q\bar{q}\mu\bar{\nu}_\mu: q\bar{q}\tau\bar{\nu}_\tau: q\bar{q}q\bar{q} \approx 1:1:8:0.05$. If the requirement of exclusivity with the other W^+W^- event selections is removed, this selection attains an efficiency (relative to all $W^+W^- \rightarrow q\bar{q}\ell\bar{\nu}_\ell$ decays) of about 40%, selecting approximately equal proportions of all $W^+W^- \rightarrow q\bar{q}\ell\bar{\nu}_\ell$ decays.

The systematic uncertainty of 2.6% on the selection efficiency is estimated by comparing data and Monte Carlo samples of mixed events, as in Section 4, and by comparing different Monte Carlo models [11, 14, 20–22]. The systematic uncertainties on the accepted background cross-section are estimated by comparing the predictions of different models [11, 22, 23], high statistics LEP1 data with that simulated by JETSET, data and Monte Carlo at $\sqrt{s} = 133$ GeV and background enriched samples at $\sqrt{s} = 161$ GeV. Systematic uncertainties on the four-fermion background are estimated using grc4f and EXCALIBUR. The systematic uncertainties of both selection efficiency and accepted background cross-section include a component from finite Monte Carlo statistics.

6 $W^+W^- \rightarrow \ell^+\nu_\ell\ell'^-\bar{\nu}_{\ell'}$ Event Selection

Approximately 11% of W pairs produced may be observed as an acoplanar pair of charged leptons with missing momentum. This analysis is sensitive to the six possible classes of observed leptons, e^+e^- , $\mu^+\mu^-$, $\tau^+\tau^-$, $e^\pm\mu^\mp$, $e^\pm\tau^\mp$, $\mu^\pm\tau^\mp$, expected to be produced in the ratio 1:1:1:2:2:2. The main backgrounds are leptonic decays in $e^+e^- \rightarrow Z^0Z^0$, $e^+e^- \rightarrow Z^0e^+e^-$ and $e^+e^- \rightarrow We\bar{\nu}_e$ processes, and $e^+e^- \rightarrow \tau^+\tau^-$. The experimental signature depends on the number of stable leptons in the final state and the amount of background depends on whether or not the leptons are of the same flavour. Therefore several selections, each designed to select a particular di-lepton class, are described. Electrons and muons are identified as in Section 4.

Cone jets³ [27] are formed in low multiplicity events [28] having between two and six tracks, and fewer than 13 charged tracks plus electromagnetic clusters. Two- and three-jet events are selected: two jets are required to contain tracks, and at least one of these jets should also include an electromagnetic cluster. At most one other jet without any tracks is accepted to allow for photon radiation. Vetoes are made against events which are consistent with $Z^0/\gamma \rightarrow \ell^+\ell^-$ or with having a hard initial state photon in the detector, events which have muons close to the beam axis, or jets with the same charge.

Two-jet events must be consistent with a di-lepton having significant missing energy and transverse momentum. One jet must have $|\cos\theta| < 0.96$ and the other $|\cos\theta| < 0.90$, their opening angle must be less than 170° , all tracks in the event must be associated with a jet, and events without identified electrons or muons must have electromagnetic clusters present in both jets. Acoplanarity, ϕ_{acop} , is defined as 180° minus the di-jet opening angle in the $r - \phi$ plane. Events with $\phi_{\text{acop}} > 60^\circ$ must have $|\cos\theta_{\text{miss}}| < 0.90$. For events with $\phi_{\text{acop}} < 60^\circ$, the component of the transverse momentum perpendicular to the event thrust axis⁴, a_t^{miss} , and the direction of the associated missing momentum, θ_a^{miss} , are required to satisfy $a_t^{\text{miss}}/E_{\text{beam}} > 0.025$ and $|\cos\theta_a^{\text{miss}}| < 0.99$. Here E_{beam} is the beam energy, $\theta_a^{\text{miss}} = \tan^{-1}(a_t^{\text{miss}}/p_z^{\text{miss}})$ and $-p_z^{\text{miss}}$ is the longitudinal missing momentum [29].

³The cone jet parameters used are a minimum energy of 2.5 GeV and cone half angle of 20° .

⁴This reduces the sensitivity to neutrinos from tau decays or poorly measured particles.

Events are finally selected if they satisfy all criteria in any of the categories defined in Table 2. Events may be selected by up to three independent selections. Category A is optimised for e^+e^- , $\mu^+\mu^-$ and $e^\pm\mu^\mp$ events and is independent of lepton identification, category B is based on significant missing transverse energy and requires at least one identified e or μ , and category C is based on identification of the di-lepton classes. C is further subdivided into four exclusive categories: C1 requires two e or two μ , C2 requires there to be no e or μ identified, C3 requires one e and one μ , while C4 requires one jet to be identified as e or μ and the other not to be identified.

Three-jet events must have fewer than five tracks, be aplanar, have at least one identified e or μ , satisfy $|\cos\theta_{\text{miss}}| < 0.90$, have a transverse momentum greater than $0.2E_{\text{beam}}$, and be kinematically inconsistent with a $\tau\tau\gamma$ final state [30]. The total energy of the jet with no charged tracks and the closer of the other jets must exceed $0.35E_{\text{beam}}$.

The distributions of ϕ_{acop} vs. x_T and x_T before applying the kinematic cuts of Table 2 are shown in Figure 2 (c) and (d), respectively. The quantity x_T is the transverse momentum of the event scaled by the beam energy. The number of candidate events selected (one $\mu^+\nu_\mu\mu^-\bar{\nu}_\mu$ and one $\mu^+\nu_\mu e^-\bar{\nu}_e$) and the corresponding Monte Carlo expectations for signal and background events are given in Table 1. The overall efficiency for selecting $W^+W^- \rightarrow \ell^+\nu_\ell\ell'^-\bar{\nu}_{\ell'}$ events is $(65.4 \pm 2.0)\%$. The efficiency and background estimates have been corrected by a multiplicative factor of 0.959 ± 0.015 to account for effects in the data not modelled in the Monte Carlo, such as detector occupancy due to off-momentum beam particles. A correction of -0.9% for modelling of final state radiation has also been included.

The systematic uncertainty of 2% on the selection efficiency is estimated by comparing W^+W^- events simulated by various Monte Carlo models [11,14,20,21] and contains a component from the correction for modelling of final state radiation. The systematic uncertainty on the accepted background cross-section is obtained by comparing different Monte Carlo models. Systematic uncertainties on both signal efficiency and accepted background cross-section include contributions from the correction for effects not modelled in the Monte Carlo and from finite Monte Carlo statistics.

7 Results

A proper treatment of the interfering four-fermion processes is desirable in extracting the W mass and production cross-section from the observed event yields. This is included explicitly in the measurement of the W mass described in Section 7.2 below, making use of the predictions of the grc4f program to account for these effects. This technique also inherently takes account of the W-mass dependence of the experimental selection cuts. In making the measurement, Standard Model expectations for four-fermion processes and branching ratios are assumed.

Since the four-fermion interference effects and mass dependence of the acceptance are expected to be small at the current level of precision, an alternative approach is also used to extract the W-pair (“CC03”) production cross-section from the data directly, neglecting the W-mass dependent effects and absorbing the interference into a mass-independent background. This division into CC03 signal events and background terms is shown in Table 1, for a representative W mass of 80.33 GeV [1] and a beam energy of 80.65 GeV. The data are consistent with the Monte Carlo expectation. The dominant systematic uncertainties in the expected number of signal events are due to the current errors of ± 0.15 GeV [1] in M_W and ± 0.10 GeV in E_{beam} [13] (8.5% and 5.9%, respectively). A W^+W^- cross-section of 3.77 pb from GENTLE was used, with an error of ± 0.08 pb which accommodates the predictions of grc4f, PYTHIA and KORALW. Uncertainties in the selection efficiencies, accepted background cross-sections and luminosity have been described in Sections 2–6.

7.1 W^+W^- production cross-section

The W^+W^- cross-section is measured using the information from the five separate channels. For each channel i , the probability of obtaining the number of observed events is calculated as a function of the W^+W^- cross-section, σ_{WW} , using Poisson statistics and assuming Standard Model branching ratios. The likelihood \mathcal{L} is formed from the product of the Poisson probabilities \mathcal{P}_i of observing N_i events for a Monte Carlo prediction of $\mu_i(\sigma_{WW})$ events:

$$\mathcal{L} = \prod_i \mathcal{P}_i(N_i, \mu_i(\sigma_{WW})) = \prod_i \frac{\mu_i(\sigma_{WW})^{N_i} e^{-\mu_i(\sigma_{WW})}}{N_i!}. \quad (1)$$

The maximum likelihood value yields the measurement of the CC03 cross-section, of

$$\sigma_{WW} = 3.62_{-0.82}^{+0.93} \pm 0.16 \text{ pb},$$

where the first uncertainty is statistical and the second systematic. From the maximum value of the likelihood curve, the level of consistency between the observed and expected number of events is 21%. The systematic uncertainty is evaluated by means of repeated Monte Carlo trials. For each trial the expected number of events in each channel is smeared according to its Gaussian uncertainty, and the corresponding cross-section value re-evaluated. The r.m.s. of this distribution was taken as the systematic uncertainty. This procedure takes into account the correlated luminosity uncertainties and small correlated systematic uncertainties between the $q\bar{q}\ell\bar{\nu}_\ell$ channels. The above result is in agreement with that obtained by taking the total number of observed events, subtracting the total expected background cross-section and dividing by the overall selection efficiency of $(60.6 \pm 0.7)\%$, which gives $\sigma_{WW} = 3.83_{-0.84}^{+0.95}$ pb.

7.2 Determination of the W boson mass

The W mass dependence of the four-fermion cross-section accepted by the selections described in this letter is determined using the grc4f generator. Events are simulated at seven different values of M_W for all processes which give the same four-fermion states as W^+W^- production, *i.e.* $q\bar{q}q\bar{q}$, $q\bar{q}\ell\bar{\nu}_\ell$ and $\ell^+\nu_\ell\ell'^-\bar{\nu}_{\ell'}$. The accepted cross-sections of non-interfering background processes, which have negligible W mass dependence, are evaluated at a single M_W using grc4f and other generators [11, 12, 14–23]. For each W^+W^- decay channel, i , the accepted cross-section is predicted as a function of $M_W - E_{\text{beam}}$ and parametrised by a second order polynomial, $\sigma_i^{\text{acc}}(M_W - E_{\text{beam}})$, using these Monte Carlo samples. The Monte Carlo predictions and parametrisations are shown in Figure 3(a).

To determine the value of M_W and its statistical uncertainty, a likelihood analogous to Equation 1 is constructed. The Monte Carlo prediction is now a direct function of $M_W - E_{\text{beam}}$, and is given by $\mu_i(M_W - E_{\text{beam}}) = \text{luminosity} \times \sigma_i^{\text{acc}}(M_W - E_{\text{beam}})$. A maximum likelihood fit is performed to extract M_W , taking into account the correlations between the $q\bar{q}\ell\bar{\nu}_\ell$ channels and assuming Standard Model branching ratios. The systematic uncertainty on the derived M_W is again obtained by means of repeated Monte Carlo trials, smearing the expected number of events in each decay channel by their corresponding uncertainties, and taking into account the correlations. The likelihood, and the M_W values from the trials, are shown in Figure 3(b) and (c), respectively. The W boson mass determined in this way is

$$M_W = 80.40_{-0.41}^{+0.44+0.09} \pm 0.10 \text{ GeV},$$

where the first and second uncertainties are statistical and systematic, respectively, and the third arises from the current estimate of the beam energy uncertainty [13].

A value of M_W can also be determined from the CC03 cross-section measurement described above. The semi-analytic program GENTLE is used to derive the dependence of σ_{WW} on M_W . The W^+W^-

cross-section and M_W measured in the CC03 framework are shown in Figure 4, together with the GENTLE prediction for $\sqrt{s} = 161.3$ GeV. The measurement obtained is $M_W = 80.40 \pm 0.43 \pm 0.09 \pm 0.10$ GeV, where the first error is statistical and the second is systematic, including all uncertainties in the cross-section measurement and an additional component to allow for differences in the σ_{WW} cross-section predicted by different programs. The third error arises from the current estimate of the beam energy uncertainty. In deriving this M_W , it has been assumed that the experimental acceptance does not vary significantly within this range of M_W values. This measurement of M_W agrees with the value determined in the full four-fermion analysis, as illustrated in Figure 4.

8 Conclusions

This letter has described the first observation of W boson pair production at centre-of-mass energies $\sqrt{s} = 161.3$ GeV in the OPAL detector at LEP. The analysis is sensitive to all expected W^+W^- decay channels. A total of 28 events have been observed for an integrated luminosity of 9.89 ± 0.06 pb $^{-1}$. This is consistent with the Standard Model expectation of 22.6 ± 2.4 signal events, assuming $M_W = 80.33$ GeV [1], and 5.0 ± 0.6 background events, where only the W^+W^- four-fermion diagrams have been considered as signal.

The observed number of events can be used to evaluate the W^+W^- (CC03) production cross-section, giving

$$\sigma_{WW} = 3.62_{-0.82}^{+0.93} \pm 0.16 \text{ pb},$$

where the uncertainties are statistical and systematic, respectively. In evaluating this cross-section, it is assumed that the four-fermion cross-section can be subdivided into W^+W^- and non- W^+W^- contributions.

From an analysis of the expected W boson mass dependence of the number of selected events, taking into account interference in the four-fermion final states, the measurement

$$M_W = 80.40_{-0.41-0.10}^{+0.44+0.09} \pm 0.10 \text{ GeV}$$

is obtained, where the first and second uncertainties are statistical and systematic, respectively, and the third arises from the beam energy uncertainty [13]. Further studies may modify the beam energy and reduce its uncertainty, which would change the measured M_W value by the same amount in the same direction. It has been verified that this assumption is correct to within 4%. This M_W is in good agreement with the world-average measurement of $M_W = 80.33 \pm 0.15$ GeV [1].

Acknowledgements

We particularly wish to thank the SL Division for the efficient operation of the LEP accelerator at the new energy of $\sqrt{s} = 161$ GeV and for their continuing close cooperation with our experimental group. We thank our colleagues from CEA, DAPNIA/SPP, CE-Saclay for their efforts over the years on the time-of-flight and trigger systems which we continue to use. In addition to the support staff at our own institutions we are pleased to acknowledge the Department of Energy, USA, National Science Foundation, USA, Particle Physics and Astronomy Research Council, UK,

Natural Sciences and Engineering Research Council, Canada,
Israel Science Foundation, administered by the Israel Academy of Science and Humanities,
Minerva Gesellschaft,
Japanese Ministry of Education, Science and Culture (the Monbusho) and a grant under the Mon-
busho International Science Research Program,
German Israeli Bi-national Science Foundation (GIF),
Bundesministerium für Bildung, Wissenschaft, Forschung und Technologie, Germany,
National Research Council of Canada,
Hungarian Foundation for Scientific Research, OTKA T-016660, and OTKA F-015089.

Selection	Expected signal	Expected background	Observed
$W^+W^- \rightarrow q\bar{q}q\bar{q}$	9.6 ± 1.0	3.44 ± 0.39	14
$W^+W^- \rightarrow q\bar{q}e\bar{\nu}_e$	3.89 ± 0.44	0.18 ± 0.27	3
$W^+W^- \rightarrow q\bar{q}\mu\bar{\nu}_\mu$	4.19 ± 0.46	0.27 ± 0.15	2
$W^+W^- \rightarrow q\bar{q}\tau\bar{\nu}_\tau$	2.32 ± 0.28	0.96 ± 0.34	7
$W^+W^- \rightarrow \ell^+\nu_\ell\ell'^-\bar{\nu}_{\ell'}$	2.58 ± 0.28	$0.19^{+0.12}_{-0.04}$	2
Combined	22.6 ± 2.4	5.0 ± 0.6	28

Table 1: Observed number of candidate events in each W^+W^- decay channel for an integrated luminosity of $9.89 \pm 0.06 \text{ pb}^{-1}$ at $161.3 \pm 0.2 \text{ GeV}$, together with expected numbers of signal and background, taking $M_W = 80.33 \pm 0.15 \text{ GeV}$. The predicted numbers for signal include systematic uncertainties from the efficiency, luminosity, beam energy and M_W uncertainties, while the background estimate includes selection and luminosity uncertainties.

Observable	Category					
	A	B	C1	C2	C3	C4
Lepton identification required	None	> 1 e or μ	ee or $\mu\mu$	no e or μ	1 e and 1 μ	1 e or 1 μ not both
ϕ_{acop} (degrees)	> 7.5	> 20.0	> 7.5	> 15.0	> 5.0	> 7.5
x_T	> 0.08	> 0.20	> 0.08	> 0.08	–	> 0.08
x_1	> $0.75 - x_2$	–	> 0.35	> 0.20	> 0.35	> 0.35
x_2	> 0.325	–	> 0.10	> 0.10	> 0.05	> 0.05
$m_{\ell\ell}$ (GeV)	–	> 10.0	> 10.0	> 10.0	–	–
$ m_{\text{recoil}} - M_{Z^0} $ (GeV)	–	> $3\Gamma_Z$	> $3\Gamma_Z$	–	–	–

Table 2: Di-jet analysis kinematic cut values for the $W^+W^- \rightarrow \ell^+\nu_\ell\ell'^-\bar{\nu}_{\ell'}$ selection, where: ϕ_{acop} is the di-jet acoplanarity angle, x_T is the transverse momentum of the event scaled by the beam energy, $x_{1(2)}$ is the energy of the more (less) energetic jet scaled by the beam energy, $m_{\ell\ell}$ is the di-lepton mass, and m_{recoil} its recoil mass. The Z^0 mass and width are taken to be $M_{Z^0} = 91.19 \text{ GeV}$ and $\Gamma_Z = 2.5 \text{ GeV}$ respectively.

References

- [1] The Particle Data Group, R.M. Barnett *et al.*, Phys. Rev. **D54** (1996) 1;
CDF Collaboration, F. Abe *et al.*, Phys. Rev. Lett. **75** (1995) 11, Phys. Rev. **D52** (1995) 4784;
CDF Collaboration, F. Abe *et al.*, Phys. Rev. Lett. **65** (1990) 2243, Phys. Rev. **D43** (1991) 2070;
UA2 Collaboration, J. Alitti *et al.*, Phys. Lett. **B276** (1992) 354;
UA1 Collaboration, C. Albajar *et al.*, Z. Phys. **C44** (1989) 15.
- [2] D0 Collaboration, S. Abachi *et al.*, Phys. Rev. Lett. **77** (1996) 3309.
- [3] Proceedings of CERN LEP2 Workshop, CERN 96-01,
W. Beenakker *et al.*, eds. G. Altarelli, F. Zwirner, February 1996, p. 79.
- [4] Proceedings of CERN LEP2 Workshop, CERN 96-01,
Z. Kunszt *et al.*, eds. G. Altarelli, F. Zwirner, February 1996, p. 141.
- [5] OPAL Collaboration, K. Ahmet *et al.*, Nucl. Instr. Meth. **A305** (1991) 275; P.P. Allport *et al.*,
Nucl. Instr. Meth. **A324** (1993) 34; P.P. Allport *et al.*, Nucl. Instr. Meth. **A346** (1994) 476.
- [6] B.E. Anderson *et al.*, IEEE Transactions on Nuclear Science, **41** (1994) 845.
- [7] OPAL Collaboration, G. Alexander *et al.*, CERN-PPE/96-047, to be published in Z. Phys. **C**.
- [8] OPAL Collaboration, G. Alexander *et al.*, Phys. Lett. **B386** (1996) 463.
- [9] OPAL Collaboration, G. Alexander *et al.*, Phys. Lett. **B376** (1996) 232.
- [10] J. Allison *et al.*, Nucl. Instr. Meth. **A317** (1992) 47.
- [11] T. Sjöstrand, Comput. Phys. Commun. **82** (1994) 74.
- [12] D. Bardin *et al.*, Nucl. Phys. B, Proc. Suppl. **37B** (1994) 148-157.
- [13] LEP Energy Working Group, private communication.
- [14] J. Fujimoto *et al.*, KEK-CP-046 (unpublished).
- [15] S. Jadach *et al.*, Comput. Phys. Commun. **79** (1994) 503.
- [16] S. Jadach, W. Placzek, B.F.L. Ward, UTHEP-95-1001, submitted to Phys. Lett.
- [17] R. Engel and J. Ranft, Phys. Rev. **D54** (1996) 4244;
R. Engel, Z. Phys. **C66** (1995) 203.
- [18] J.A.M. Vermaseren, Nucl. Phys. **B229** (1983) 347.
- [19] G. Montagna *et al.*, Nucl. Phys. **B452** (1996) 161.
- [20] Program KORALW, M. Skrzypek *et al.*, Comput. Phys. Commun. **94** (1996) 216;
M. Skrzypek *et al.*, Phys. Lett. **B372** (1996) 289.
- [21] Program EXCALIBUR, F.A. Berends, R. Pittau and R. Kleiss, Comput. Phys. Commun. **85**
(1995) 437.
- [22] Program HERWIG, G. Marchesini *et al.*, Comput. Phys. Commun. **67** (1992) 465.
- [23] Program ARIADNE, L. Lönnblad, Comput. Phys. Commun. **71** (1992) 15.
- [24] OPAL Collaboration, G. Alexander *et al.*, Z. Phys. **C52** (1991) 175.

- [25] N. Brown and W.J. Stirling, Phys. Lett. **B252** (1990) 657;
S. Bethke, Z. Kunszt, D. Soper and W.J. Stirling, Nucl. Phys. **B370** (1992) 310;
S. Catani *et al.*, Phys. Lett. **B269** (1991) 432;
N. Brown and W.J. Stirling, Z. Phys. **C53** (1992) 629.
- [26] OPAL Collaboration, M.Z. Akrawy *et al.*, Phys. Lett. **B253** (1990) 511.
- [27] OPAL Collaboration, R. Akers *et al.*, Z. Phys. **C63** (1994) 197.
- [28] OPAL Collaboration, M.Z. Akrawy *et al.*, Phys. Lett. **B235** (1990) 379.
- [29] OPAL Collaboration, G. Alexander *et al.*, CERN-PPE/96-096, to be published in Z. Phys. **C**.
- [30] OPAL Collaboration, G. Alexander *et al.*, Phys. Lett. **B377** (1996) 181.

OPAL

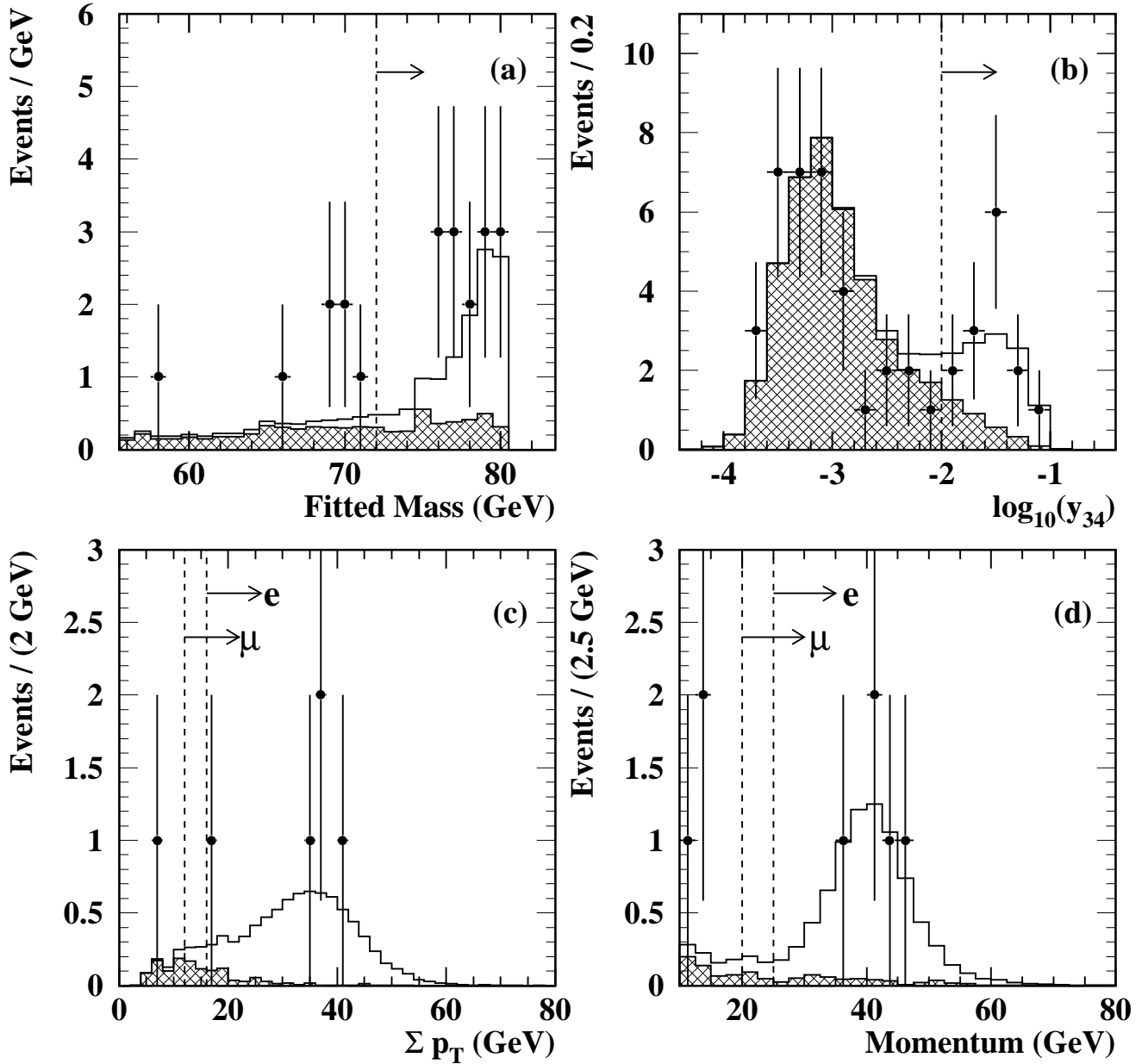


Figure 1: Illustration of the selection quantities described in Sections 3 and 4 with Monte Carlo signal and background events: (a) the kinematic fit mass and (b) $\log y_{34}$ for the $W^+W^- \rightarrow q\bar{q}q\bar{q}$ channel; (c) Σp_T and (d) lepton momentum for the $W^+W^- \rightarrow q\bar{q}e\bar{\nu}_e$, $q\bar{q}\mu\bar{\nu}_\mu$ channels. The pairing of jets to W candidates chosen for plot (a) is the one with the largest kinematic fit mass with a fit probability greater than 1%. Cuts are indicated with a vertical line and an arrow pointing in the direction of selected events. Each distribution is shown after all selection requirements have been applied to the other distributions. The hatched histogram shows the expected distribution of the combined background and the open histogram is the sum of the expected signal and the combined background. The data are indicated by points.

OPAL

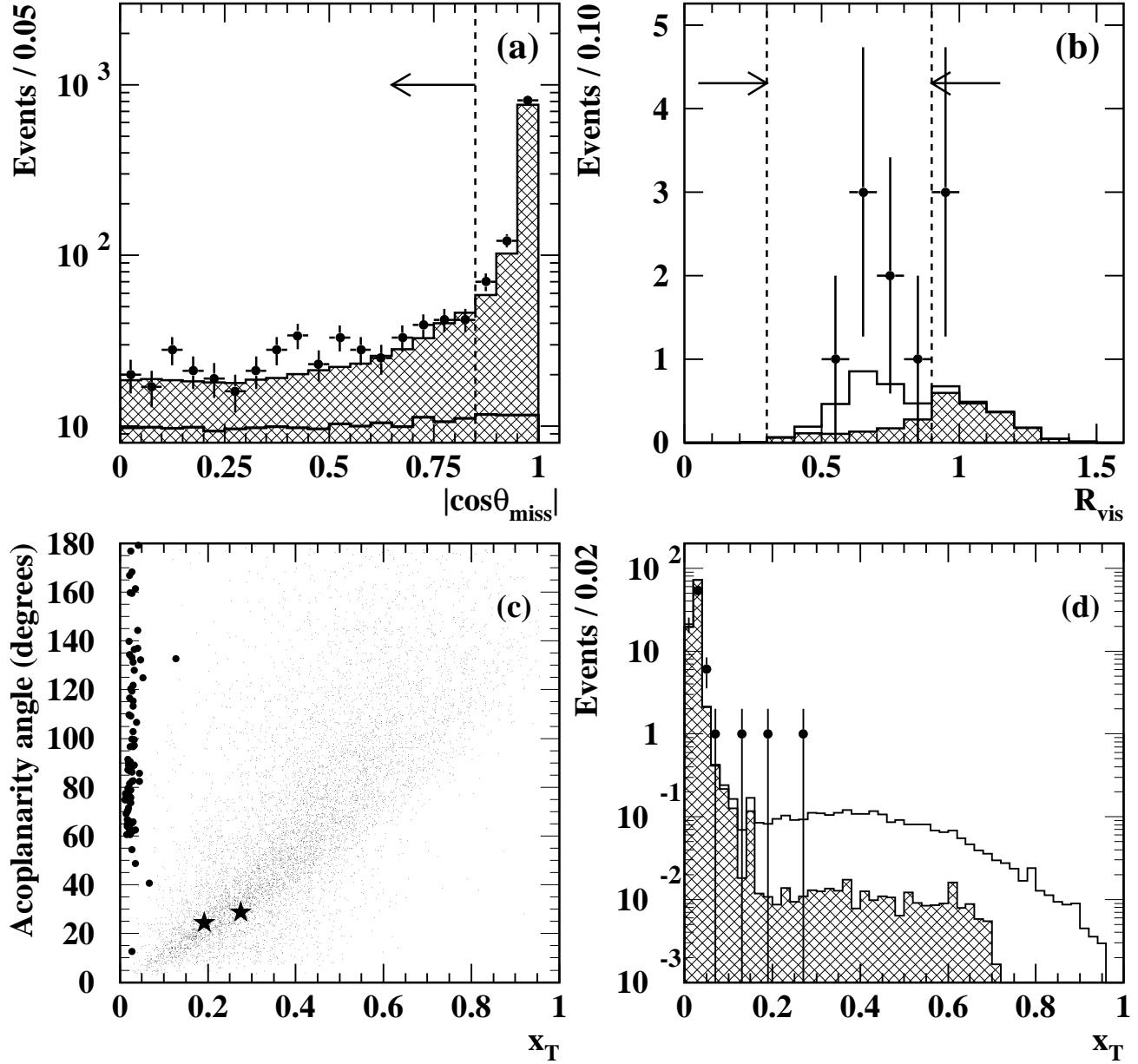


Figure 2: Illustration of the selection quantities described in Sections 5 and 6 with Monte Carlo signal and background events: (a) $|\cos\theta_{\text{miss}}|$ after multiplicity cuts only, and (b) R_{vis} after all other cuts in the $W^+W^- \rightarrow q\bar{q}\tau\bar{\nu}_\tau$ channel. The symbols are as defined in Figure 1. In (a) the W^+W^- contribution is superimposed as a solid line and scaled up by a factor of 30. Plot (c) illustrates ϕ_{acop} vs. x_T for selected di-jet events in the $W^+W^- \rightarrow \ell^+\nu_\ell\ell'^-\bar{\nu}_{\ell'}$ channel prior to applying the kinematic criteria. The large points are events in the data, the small points represent simulated W pair events. The two events accepted after all cuts are shown as stars. Plot (d) shows the projection of the x_T distribution, with symbols as defined in Figure 1.

OPAL

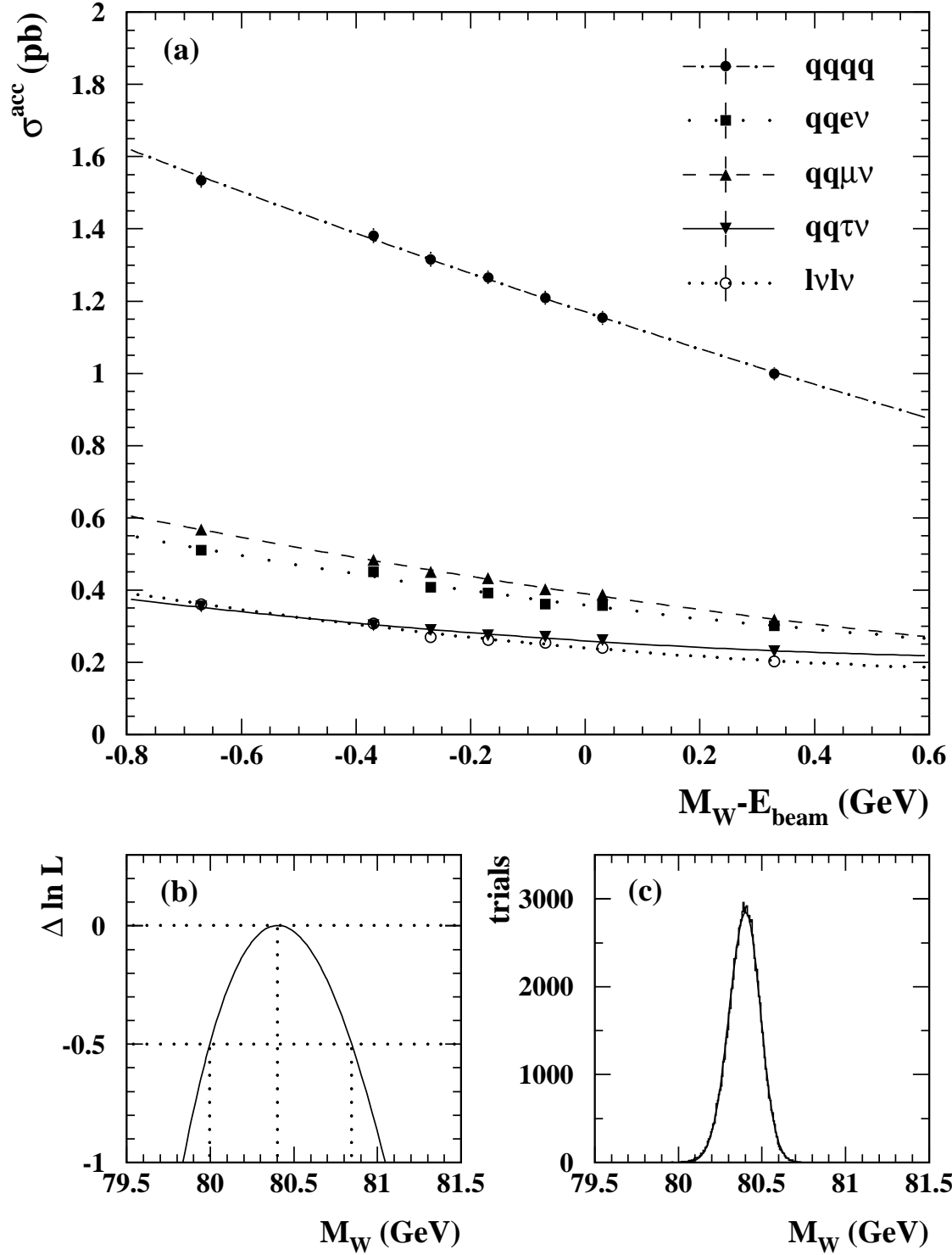


Figure 3: The accepted cross-sections in each W^+W^- decay channel as a function of $M_W - E_{\text{beam}}$ are illustrated in (a), using the event generators described in the text. In each case, this is parametrised by a second order polynomial. The likelihood function and the corresponding statistical uncertainty are shown in (b) for $\sqrt{s} = 161.3$ GeV. Plot (c) shows the distribution of M_W values evaluated using repeated Monte Carlo trials. Its width gives the systematic uncertainty.

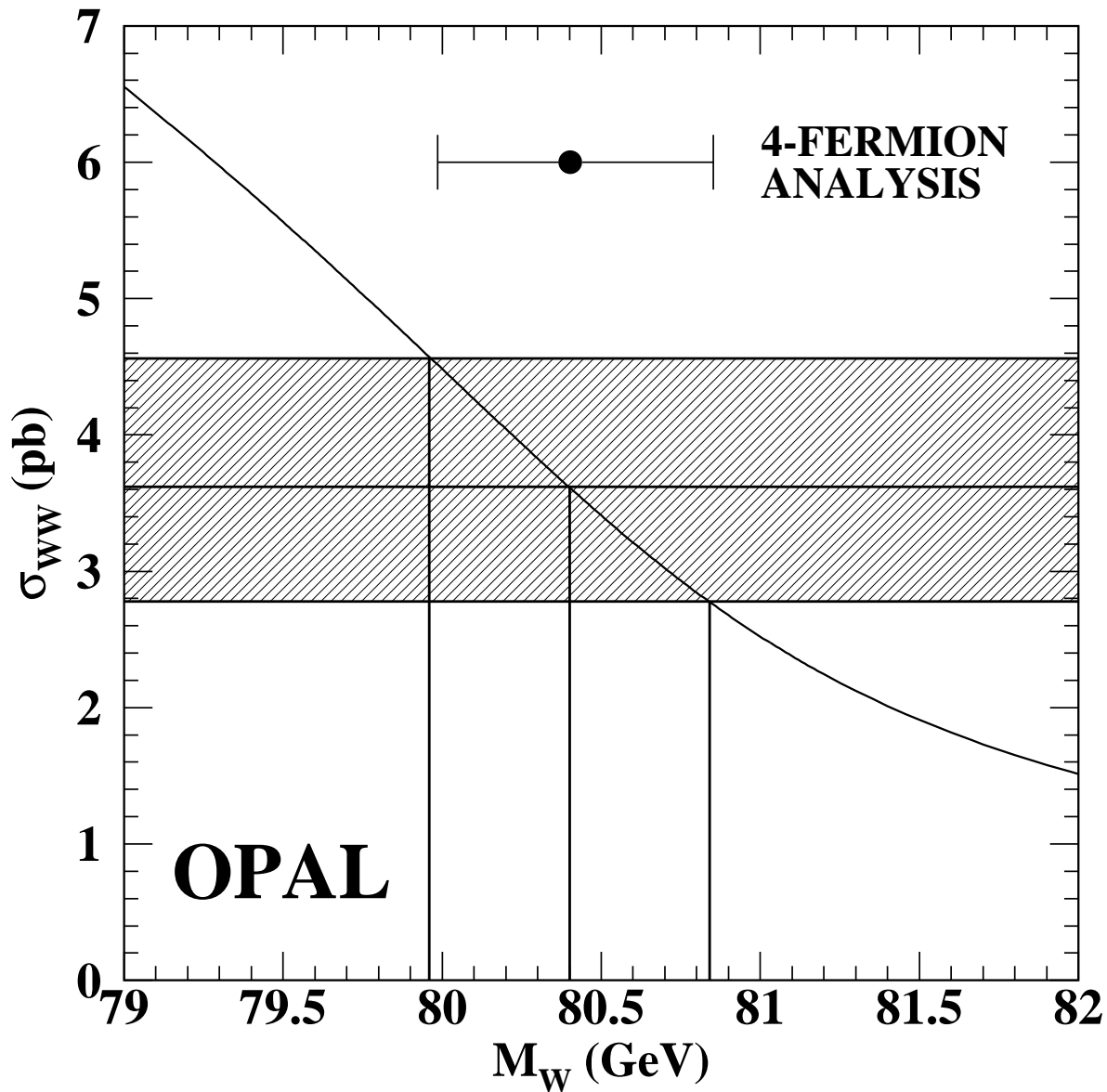


Figure 4: Distribution of σ_{WW} as a function of M_W , as predicted by GENTLE for $\sqrt{s} = 161.3$ GeV. The measured W^+W^- cross-section is shown by a shaded band and the corresponding W boson mass by vertical lines. The principal measurement of M_W in this letter is shown as a point with error bars. The uncertainties include statistical and systematic contributions, but do not include the effect of the beam energy uncertainty.